Therapeutics and Clinical Risk Management

Dovepress
Taylor & Francis Group

Open Access Full Text Article

ORIGINAL RESEARCH

Predictive Value of CT Fractional Flow Reserve and Fat Attenuation Index Derived from Coronary CT Angiography for In-Stent Restenosis After Percutaneous Coronary Intervention

Beibei Li[1,2], Zhiguo Zhang[2], Xianglei Wei[2], Tianzeng Song[3], Yi Zhao[4], Wei Wang[4]

[1]Graduate School of Dalian Medical University, Dalian, Liaoning, 116000, People's Republic of China; [2]Department of Radiology, Linyi Central Hospital, Yishui County, Linyi, Shandong, 276400, People's Republic of China; [3]Department of Orthopeadic Surgery, Linyi Central Hospital, Yishui County, Linyi, Shandong, 276400, People's Republic of China; [4]Department of Radiology, Affiliated Hospital of Yangzhou University, Yangzhou, Jiangsu, 225000, People's Republic of China

Correspondence: Wei Wang, Email waywang@126.com

Aim: To investigate the predictive value of CT fractional flow reserve (CT-FFR) and fat attenuation index (FAI) based on Coronary CT Angiography (CCTA) for in-stent restenosis (ISR) in patients with CAD after PCI.

Methods: Patients with coronary heart disease who were followed up after coronary stent implantation were retrospectively collected, and clinical data, stent features and imaging characteristics were recorded. The Spearman test was used to analyze the correlation between CT-FFR, FAI and ISR. Univariate and multivariate logistic regression were used to determine the independent influencing factors of ISR, and a nomogram model was constructed.

Results: A total of 378 patients were ultimately included. Among them, there were 120 cases in the ISR group and 258 cases in the non-ISR group. Multivariate analysis revealed that $CT\text{-}FFR_{2cm}$, ΔCT-FFR, FAI_{lesion}, stent length, ΔCT-FFR/length, hyperlipidemia, and lipoprotein(a) are independent predictors of ISR. The ROC analysis demonstrated that ΔCT-FFR had the highest predictive accuracy for ISR, with an AUC of 0.923 (95% CI: 0.889–0.957). Several clinical prediction models were developed, among which Model 3 displayed the highest predictive performance (AUC: 0.958, 95% CI, 0.932–0.984). A statistically significant difference was observed between Model 1 and Model 2 (AUC: 0.925 vs 0.950, $P < 0.05$). However, no significant difference was found between Model 1 and Model 3 (AUC: 0.925 vs 0.928, $P > 0.05$).

Conclusion: ΔCT-FFR and peri-stent FAI, as independent predictors of ISR after PCI in patients with coronary heart disease, have a high predictive value for ISR. In addition, the FAI around the stent has incremental value for CT-FFR. It is worth noting that, compared with clinical data, imaging features show higher predictive value.

Keywords: coronary CT angiography, CT fractional flow reserve, perivascular fat attenuation index, coronary heart disease, in-stent restenosis

Introduction

Coronary heart disease is the leading cause of death worldwide, accounting for approximately 30% of all deaths.[1] Percutaneous coronary intervention (PCI) can directly implant stents in the most severely narrowed coronary arteries to improve the degree of coronary artery stenosis. It has the characteristics of rapidly restoring myocardial blood and oxygen supply and thereby improving the clinical symptoms of patients, and has become the most effective means of treating coronary heart disease.[2,3] However, in-stent restenosis (ISR) reduces the overall effectiveness of PCI. Although the incidence of ISR in bare-metal stents is 30% at 6 months, and that in drug-eluting stents (DES) drops to 7% at 4 years,[4] ISR remains the main cause of long-term failure after PCI.[5] A 10-year data from a DES randomized trial showed that ISR led to a target lesion revascularization rate of approximately 20% at 10 years.[6] A study by Seiler et al demonstrated that at 1-year follow-up, the

Received: 16 July 2025
Accepted: 26 October 2025
Published: 3 November 2025

MACE rate after ISR treatment was 19.7%; 15.4% of patients experienced TVF (target vessel failure), with myocardial infarction (MI) and stent thrombosis occurring in 5.9% and 2.1% of patients, respectively.[7] Another study has demonstrated that the rate of target vessel revascularization due to in-stent restenosis three years after drug-eluting stent implantation reached 5.2%.[8] Therefore, early identification and control of related risk factors are key approaches to reducing the incidence of ISR and improving patient prognosis.

Fractional Flow Reserve (FFR) is an invasive diagnostic technique widely regarded as the "gold standard" for assessing the hemodynamic significance of coronary artery lesions. It effectively quantifies the extent of myocardial ischemia, offers clinical guidance on the necessity of stent implantation during PCI, and aids in predicting patient outcomes following PCI.[9] Previous studies have shown that FFR has certain value in the diagnosis and prognosis assessment of ISR.[10] However, its invasive nature, high cost, large radiation dose and adverse reactions have limited its clinical application. Therefore, a non-invasive CT-based fractional flow reserve (CT-FFR) has emerged. CT-FFR is obtained through computational fluid dynamics (CFD) simulation,[11] and in recent years, CT-FFR software based on machine learning (ML) algorithms has gradually matured.[12] Existing studies have demonstrated that CT-FFR has a good correlation with invasive FFR in identifying ISR (OR = 0.84).[13]

Inflammation plays a significant role in the occurrence and development of ISR. Pericoronary adipose tissue (PCAT) refers to the adipose tissue that surrounds the coronary arteries and exhibits a significant bidirectional interaction with the vascular wall.[14] Fat attenuation index (FAI), a novel and non-invasive imaging biomarker based on coronary computed tomography angiography (CCTA), visualizes and quantifies the inflammation around coronary arteries by mapping the attenuation gradient of PCAT and tracking the changes in the size of local adipocytes and lipid content around coronary arteries.[15] Previous studies have shown that FAI is associated with high-risk and vulnerable plaques and has high diagnostic value for coronary artery stenosis and myocardial ischemia, and is significantly superior to CCTA alone.[16–18] Further studies have confirmed that FAI is significantly associated with adverse cardiac events and ISR, and has high predictive value.[19,20] However, the predictive value of CT-FFR combined with FAI based on deep learning for ISR after PCI and its prognostic assessment have not been systematically verified.

To explore how the fractional flow reserve and fat attenuation index around the stent affect ISR, this study proposes the following verifiable hypothesis: The CT-FFR and FAI values derived from the CCTA, are correlated with the occurrence of ISR. Therefore, this study aims to investigate the correlation between CT-FFR and FAI values derived from the CCTA deep learning method and ISR following percutaneous coronary intervention, as well as to evaluate their predictive value for ISR by integrating the functional and inflammatory parameters around the stent.

Materials and Methods

Patient Population

This was a single-center retrospective study. A retrospective collection was made of patients with coronary heart disease who underwent coronary stent implantation at Linyi Central Hospital from January 2019 to December 2024 and were readmitted for treatment due to recurrent angina pectoris and other symptoms. All patients underwent coronary CT angiography (CCTA) and invasive coronary angiography (CAG) simultaneously. Inclusion criteria were: (1) Patients who underwent both CCTA and CAG after coronary stent implantation, with an interval of ≥ 90 days, The interval between CCTA and CAG is less than two weeks; (2) Good image quality, suitable for image analysis and measurement of FAI and CT-FFR values. Exclusion criteria were: (1) Patients with incomplete clinical data; (2) Patients who did not undergo CAG or the time interval between CAG and CCTA < 90 days; (3) Patients with stents located only in the left main trunk or branches, except for the three main arteries, or stents located within 10 mm of the proximal right coronary artery; (4) Patients with congenital coronary artery anomalies or congenital heart disease; (5) Patients who underwent coronary artery bypass grafting (CABG) surgery; (6) Patients with poor image quality due to various reasons, making assessment impossible. The clinical data of patients were collected from the hospital's electronic medical record system, outpatient records, and telephone follow-up interviews. Record the patient's age, gender, height, weight, BMI, hypertension, hyperlipidemia, diabetes, smoking, drinking and laboratory test data during the CCTA examination. Laboratory tests included lipid analysis, myocardial enzyme spectrum analysis, C-reactive protein and erythrocyte sedimentation rate analysis. If a patient had multiple laboratory tests, the results

closest to CCTA were selected. Record whether the patient has achieved complete revascularization, the pharmacological therapy following revascularization, and the clinical presentation of patients, LV functions and comorbidities. Record the characteristics of the stent, including the vessel and segment where the stent is located, the diameter of the stent, the total length of the stent, the number of stents, and the overlapping situation.

CT Acquisition and Reconstruction

CCTA was performed with a third-generation dual-source CT device (Siemens SOMATOM Force). All patients signed informed consent forms. Scanning range: The upper boundary starts 2cm below the tracheal bifurcation, and the lower boundary ends above the diaphragm. The contrast dose tracking and triggering technique was used to select the ROI at the ascending aorta root, set the triggering threshold to 100 Hu, and delay 5 seconds for automatic scanning. Scanning parameters: Tube current modulation technology was adopted, and the tube voltage ranged from 70–120 kV. The interval is 0.5 mm, and the layer thickness is 0.75 mm. During the examination, the patient's electrocardiogram, heart rate, blood pressure, clinical symptoms, and other relevant parameters are continuously monitored. The procedure will be terminated if any of the following abnormalities occur: arrhythmia, a sustained decrease in heart rate, a blood pressure drop exceeding 40 mmHg compared to baseline, acute chest pain, or new-onset ST-segment elevation or depression.

CCTA Image Analysis

All CCTA images were uploaded to the post-processing workstation (Syngo.Via, Siemens), and the best diastolic images were selected for image processing. Two radiologists with more than five years of experience in coronary CTA interpretation analyzed the CCTA measurements. The CCTA measurement parameters encompass the normal lumen diameter at the proximal stent segment, the minimum lumen diameter (MLD) within the stent, and the minimum lumen area (MLA) of the stent, all derived through standardized image post-processing techniques such as multiplanar reconstruction (MPR), curved planar reconstruction (CPR), maximum intensity projection (MIP), and volume rendering technique (VRT).

CT-FFR measurement: All patients' CCTA data were uploaded to the artificial intelligence analysis software (Coronary Doc. Shukun Technology, China) in DICOM format. The software leverages artificial intelligence technology based on neural network models to learn the relationship between computational fluid dynamics (CFD) and anatomical structures, enabling the calculation of CT-FFR values for blood vessels with diameters exceeding 2 millimeters.[21,22] CT-FFR measurement includes the CT-FFR value at the proximal edge of the stent (CT-FFR_{pro}), the CT-FFR value at the minimum area of the stent (CT-FFR_{min}), the CT-FFR value at the distal edge of the stent (CT-FFR_{dis}), the CT-FFR value 2 cm from the distal edge of the stent (CT-FFR_{2cm}). Additionally, the ΔCT-FFR value was calculated as the difference between CT-FFR_{pro} and CT-FFR_{dis}. The study also recorded the rate of change of CT-FFR values relative to stent length, expressed as ΔCT-FFR per unit length (ΔCT-FFR/length).

FAI measurement: The fat area value range is from −190HU to −30HU. The radial distance of the outer wall of the coronary artery is manually modified to the length of the target vessel diameter. Based on the vessel level, the software can automatically calculate the FAI value within 40 mm of the proximal end of the three main coronary arteries of the patient. To minimize the influence of the aortic wall, the stent area placed within the 10 mm segment at the distal end of the right coronary artery was excluded in this study.[15] Based on the vessel level, the FAI value of the target vessel where the stent is located is recorded. Based on the lesion level, the length range of the stent from the proximal to the distal end (including 5 mm within the proximal and distal edges) is manually defined, and the radial distance is manually adjusted to make the diameter equal to the diameter of the stent, for the measurement of lesion-specific FAI (Lesion-specific FAI, FAI_{lesion}) around the stent.[23] Two senior radiologists, each with more than five years of experience in cardiovascular imaging diagnosis, independently performed CT-FFR and FAI analyses in a double-blind fashion, without access to clinical data or ICA results. In the event of discrepancies, a senior physician was consulted to resolve differences through consensus evaluation.

ICA Acquisition

The examination was conducted using the Philips Azurion 7 M20 angiography machine. Conventional angiography of the left and right coronary arteries was performed in various positions. Two senior cardiologists made the diagnosis of in-stent restenosis (ISR) without knowledge of the CCTA results, and the results were recorded and stored in the hospital's electronic medical record system. ISR was defined as a lumen diameter stenosis of ≥ 50% in the stent segment or its proximal or distal edge (a segment adjacent to the stent with a length of 5 mm).[24] According to ICA measurements, all patients who underwent coronary stenting were divided into two groups: vessels with ISR (ISR group) and vessels without ISR (non-ISR group).

Statistical Analysis

SPSS 26.0 and R (4.2.1) software were used for statistical analysis. Continuous data conforming to a normal distribution are presented as the means ± standard deviations and were compared between groups with the independent sample *t* test. Continuous data that were not normally distributed are expressed as medians (interquartile intervals) and were compared between groups with the Wilcoxon rank-sum test. Categorical variables are expressed as frequencies and percentages and were compared with the chi-square test. Spearman correlation analysis was employed to explore the relationships between various risk factors and ISR. Following the collinearity analysis of the research parameters, both univariate and multivariate logistic regression analyses were performed to identify independent risk factors for ISR. Subsequently, nomogram models and various clinical models were developed. The predictive performance of these models was assessed using the area under the curve (AUC) of the receiver operating characteristic curve and the concordance index (C-index). Additionally, calibration curves were employed to evaluate the agreement between predicted probabilities and observed outcomes, while decision curve analysis was conducted to determine the clinical utility of the models. A *P* value <0.05 was considered statistically significant.

Results

Patient Characteristics and Clinical Outcomes

A total of 378 patients were ultimately included in this study. Among them, 120 cases were included in the ISR group (31.7%), 88 were male (73.3%), and the age was 65.05 ± 8.58 (years). A total of 258 cases were included in the non-ISR group (68.3%), with 176 males (68.2%) and an age of 63.36 ± 8.71 (years). The flow chart is shown in Figure 1. There were statistically significant differences between the two patient groups with respect to hyperlipidemia, lipoprotein(a), hydroxybutyrate dehydrogenase, troponin, NT-proBNP levels and ACEI/ARB. The results of the blood vessels where the stents were located showed that there were 218 cases (57.7%) of LAD, 69 cases (18.2%) of LCX, and 91 cases (24.1%) of RCA. The results of the stent segments showed that there were 143 cases (37.8%) in the proximal segment, 90 cases (23.8%) in the proximal and middle segments, 82 cases (21.7%) in the middle segment, and 63 cases (16.7%) in the distal segment. There were statistically significant differences in stent length, number of stents, stent diameter, minimum stent lumen area, and minimum lumen diameter between the two groups ($P < 0.05$). There was no statistically significant difference in the diameter of normal blood vessels in the proximal segment of the stent and the overlapping stents. There were statistically significant differences in CT-FFR_{pro}, CT-FFR_{min}, CT-FFR_{dis}, CT-FFR_{2cm}, ΔCT-FFR, and ΔCT-FFR /length between the two groups ($P < 0.05$). The FAI values of the target vessels and the FAI values (FAI_{lesion}) around the stents showed statistically significant differences between the two groups ($P < 0.05$). The patient and stent characteristics as well as relevant results of CCTA, CT-FFR and FAI measurements are displayed in Table 1.

Correlation Analysis of CT-FFR, FAI and ISR

According to the Spearman correlation analysis, CT-FFR_{2cm} showed a moderate negative correlation with ISR ($R = -0.60$, $P < 0.001$). ΔCT-FFR demonstrated a moderate positive correlation with ISR ($R = 0.684$, $P < 0.001$). FAI_{lesion} also exhibited a moderate positive association with ISR ($R = 0.576$, $P < 0.001$). Furthermore, ΔCT-FFR/length was moderately positively correlated with ISR ($R = 0.635$, $P < 0.001$) (Figure 2).

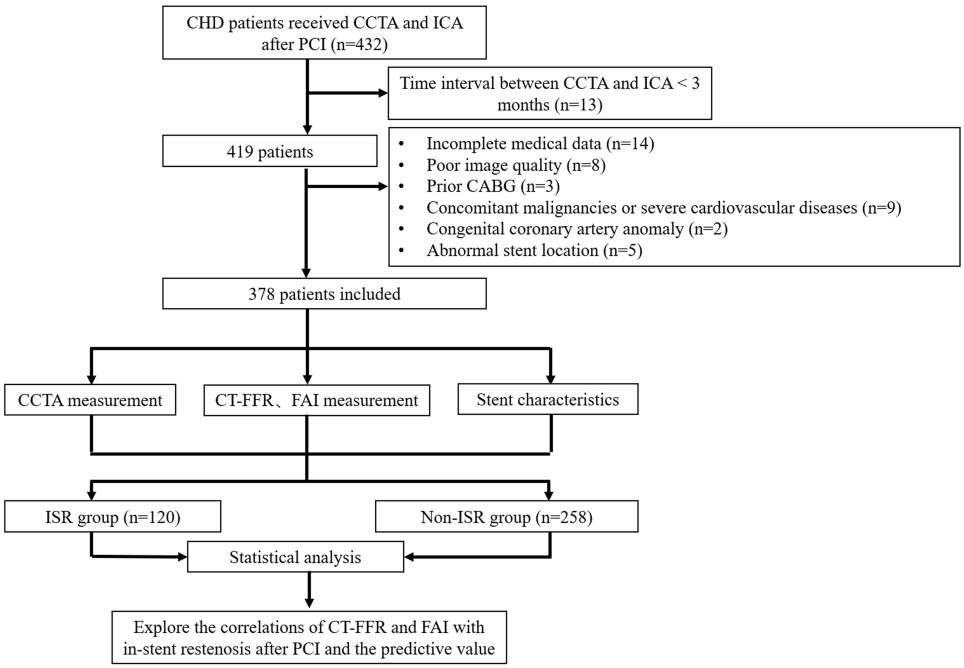

Figure 1 Flow chart of inclusion and exclusion criteria for the study population.

Univariate and Multivariate Analyses for ISR

Univariate logistic regression analysis demonstrated that CT-FFR$_{pro}$, CT-FFR$_{min}$, CT-FFR$_{dis}$, CT-FFR$_{2cm}$, ΔCT-FFR, FAI, FAI$_{lesion}$, stent length, ΔCT-FFR/length, stents number, MLD and MLA, brain natriuretic peptide precursor,

Table 1 Comparison of General Data Between the Two Groups

Characteristics	ISR	None-ISR	*P* value
n	120	258	
Sex (male), n (%)	88 (73.3%)	176 (68.2%)	0.313
Age	65.05 ± 8.58	63.36 ± 8.71	0.080
Height	169 (160, 170)	169 (160, 170)	0.936
Weight	70 (65, 75)	70 (63, 75)	0.120
BMI	24.65 (24.22, 27.06)	24.22 (23.81, 26.97)	0.229
Hypertension,n(%)	79 (65.8%)	141 (54.7%)	0.051
Diabetes,n(%)	38 (31.7%)	75 (29.1%)	0.608
Hyperlipidemia,n(%)	30 (25.0%)	19 (7.4%)	< 0.001*
Smoking,n(%)	41 (34.2%)	74 (28.7%)	0.281
Drinking,n(%)	28 (20.8%)	57 (22.1%)	0.788
TC	3.83 (3.2, 4.81)	3.78 (3.192, 4.64)	0.456
TG	1.23 (0.87, 1.93)	1.315 (0.96, 1.91)	0.522
HDL-C	1.02 (0.84, 1.2)	1.04 (0.88, 1.23)	0.466
LDL-C	2.30 (1.84, 2.87)	2.18 (1.79, 2.83)	0.245
ApoE	3.1 (2.5, 3.72)	3.1 (2.4, 3.9)	0.748
LP(a)	250 (137.75, 468)	192.5 (110.25, 325.75)	< 0.001*
AST	21 (17, 26)	20 (17, 24)	0.689
CK	81 (62, 110)	75 (54, 105.5)	0.060
LDH	195 (171, 224.75)	192 (168, 217)	0.350
HBDH	122 (108, 143.75)	118 (103, 135)	0.048*
CK-MB	1.6 (1.2, 2.07)	1.6 (1.3, 2.1)	0.863

(*Continued*)

https://doi.org/10.2147/TCRM.S554207

Table 1 (Continued).

Characteristics	ISR	None-ISR	*P* value
cTn	10.9 (7.12, 23.06)	8.715 (5.94, 14.22)	0.004*
NT-proBNP	137 (57.92, 348.25)	97.75 (39.14, 162.75)	0.001*
ESR	9 (3, 17.25)	8 (3, 16.25)	0.399
CRP	1.45 (0.83, 3.30)	1.23 (0.60, 2.75)	0.080
Antiplatelet drug,n(%)	107 (89.2%)	240 (93.0%)	0.203
Statins,n(%)	102 (85.0%)	224 (86.8%)	0.632
ACEI/ARB,n(%)	69 (57.5%)	181 (69.8%)	0.016*
BBs,n(%)	66 (55.0%)	162 (62.8%)	0.137
UA,n(%)	40 (33.3%)	71 (27.5%)	0.248
STEMI,n(%)	5 (4.2%)	5 (1.9%)	0.361
NSTEMI,n(%)	8 (6.7%)	6 (2.3%)	0.109
SAP,n(%)	67 (55.8%)	176 (68.2%)	0.054
LVF, n (%)	17 (14.2%)	27 (10.5%)	0.296
Complete revascularization, n (%)	28 (23.3%)	50 (19.4%)	0.377
Comorbidities	12 (10.0%)	18 (7.0%)	0.311
Stent length (mm)	33 (25, 42.25)	30 (22, 39)	0.037*
Stent number, n (%)	35 (29.2%)	51 (19.8%)	0.042*
Stent diameter	3 (2.75, 3)	3 (3, 3.5)	0.042*
Normal diameter	3.8 (3.3, 4.3)	3.95 (3.3, 4.5)	0.156
MLD	0.7 (0.4, 1.1)	1.5 (0.8, 2.1)	< 0.001*
MLA	1.05 (0.3, 3.83)	4.9 (1.6, 8.5)	< 0.001*
Overlap, n (%)	37 (30.8%)	59 (22.9%)	0.098
CT-FFR $_{pro}$	0.95 (0.89, 0.97)	0.96 (0.92, 0.98)	0.001*
CT-FFR $_{min}$	0.88 (0.8, 0.93)	0.94 (0.9, 0.97)	< 0.001*
CT-FFR $_{dis}$	0.82 (0.72, 0.88)	0.93 (0.88, 0.96)	< 0.001*
CT-FFR $_{2cm}$	0.76 (0.69, 0.83)	0.9 (0.85, 0.94)	< 0.001*
ΔCT-FFR	0.11 (0.09, 0.15)	0.03 (0.02, 0.05)	< 0.001*
FAI_{lesion}	−76 (−82, −69)	−87 (−91, −83)	< 0.001*
FAI	−74 (−80, −68)	−85 (−90, −78)	< 0.001*
ΔCT-FFR/length	0.32 (0.21, 0.47)	0.083 (0.05, 0.14)	< 0.001*

Note: *Significant P values (<0.05).
Abbreviations: ISR, In-Stent Restenosis; CT-FFR, Computed tomography derived fractional flow reserve; FAI, perivascular fat attenuation index.

hyperlipidemia, ACEI/ARB and lipoprotein(a) were all associated with ISR. Following collinearity assessment, CT-FFR_{pro} and CT-FFR_{dis} were excluded, due to multicollinearity. The remaining variables were entered into a multivariate logistic regression model. The results showed that CT-FFR_{2cm}, ΔCT-FFR, FAI_{lesion}, ΔCT-FFR/length, hyperlipidemia and lipoprotein a were independent predictors of ISR (Table 2).

Nomogram Construction and Prediction Performance of ISR Test Parameters

A nomogram model was developed based on the aforementioned independent influencing factors to predict the occurrence of in-stent restenosis (ISR) in patients who underwent percutaneous coronary intervention (PCI) (Figure 3). The model demonstrated high predictive accuracy, as evidenced by a C-index of 0.966. Receiver operating characteristic (ROC) curve analysis was performed to evaluate the performance of the predictive model. The results indicated that ΔCT-FFR exhibited the highest predictive value for ISR, with an AUC of 0.923 (95% CI: 0.889–0.957), outperforming both FAI_{lesion} (AUC=0.857, 95% CI: 0.817–0.896) and clinical data (AUC=0.688, 95% CI: 0.628–0.748). This difference was statistically significant ($P < 0.05$) (Figure 4). Several clinical models were constructed, and calibration and decision curve analyses were conducted to further validate the ISR prediction model. Model 1 only includes ΔCT-FFR; Model 2 includes ΔCT-FFR and FAI_{lesion}; Model 3 includes ΔCT-FFR, FAI_{lesion} and clinical data.

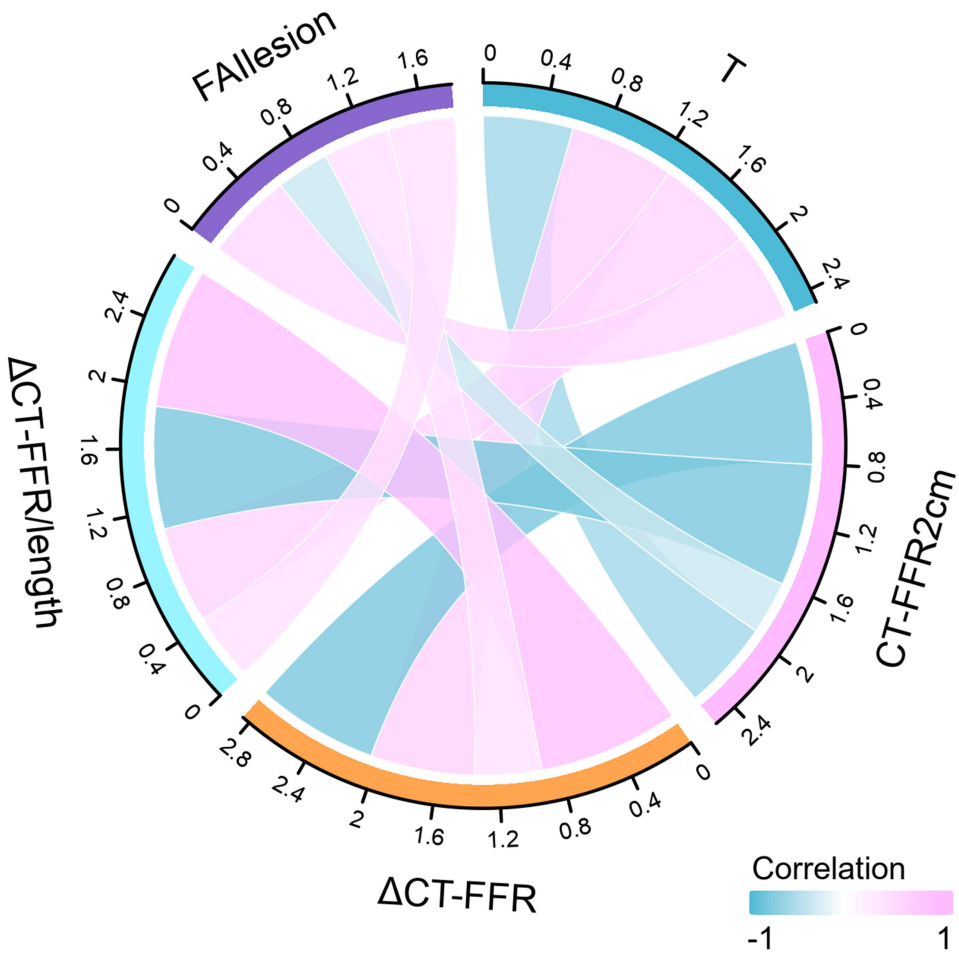

Figure 2 The correlation between various factors and in-stent restenosis after PCI.

The ROC results showed that the area under the curve (AUC), cut-off value, sensitivity, specificity, accuracy, positive predictive value (PPV), and negative predictive value (NPV) of Model 1 for predicting ISR were 0.923 (95% CI: 0.889–0.957), 0.08, 0.965, 0.783, 0.907, 0.905, and 0.913, respectively. For Model 2, the corresponding values were 0.955 (95% CI: 0.930–0.981), 0.439, 0.957, 0.858, 0.926, 0.936, and 0.904, respectively. For Model 3, these values were 0.958 (95% CI: 0.932–0.984), 0.337, 0.942, 0.892, 0.926, 0.949, and 0.877, respectively. Model 3 had the highest predictive value (AUC: 0.958, 95% CI, 0.932–0.984). There was a statistically significant difference between Model 1

Table 2 Univariate and Multivariate Logistic Regression Analysis for ISR

Characteristics	Univariate Analysis		Multivariate Analysis	
	Odds Ratio (95% CI)	*P* value	Odds Ratio (95% CI)	*P* value
$CT\text{-}FFR_{min}$	0.586(0.467–0.734)	<0.001*	1.929(1.178-0.160)	0.521
$CT\text{-}FFR_{2cm}$	0.415(0.327–0.528)	<0.001*	0.451(0.266–0.766)	0.009*
ΔCT-FFR	2.561(2.045–3.208)	<0.001*	1.412(0.806–2.471)	0.003*
FAI_{lesion}	0.820(0.785–0.857)	<0.001*	0.860(0.778–0.951)	0.003*
FAI	0.882(0.855–0.909)	<0.001*	0.998(0.919–1.085)	0.970
Stent length	0.981(0.965–0.997)	0.021*	0.998(0.938–1.062)	0.953
ΔCT-FFR/length	2.595(2.033–3.311)	<0.001*	1.895(1.009-0.559)	0.016*

(*Continued*)

https://doi.org/10.2147/TCRM.S554207

Table 2 (Continued).

Characteristics	Univariate Analysis		Multivariate Analysis	
	Odds Ratio (95% CI)	*P* value	Odds Ratio (95% CI)	*P* value
Stent number	1.671(1.015–2.752)	0.044*	0.997(0.210–4.736)	0.997
Stent diameter	1.772(0.991–3.167)	0.054		
MLD	4.110(2.775–6.086)	<0.001*	3.306(0.758–14.422)	0.112
MLA	1.286(1.191–1.389)	<0.001*	0.827(0.624–1.096)	0.187
HBDH	0.998(0.995–1.002)	0.323		
CT	0.999(0.996–1.002)	0.398		
NT-probnp	0.999(0.999–1.000)	0.005*	1.000(0.999–1.000)	0.169
CRP	0.995 (0.985–1.006)	0.378		
Hyperlipemia	0.238(0.128–0.445)	<0.001*	0.288(0.088–0.942)	0.039*
Lp(a)	0.997(0.996–0.998)	<0.001*	0.998(0.996–1.000)	0.042*
ACEI/ARB	0.576 (0.367–0.902)	0.016*	0.613 (0.345–1.089)	0.095

Note: *Significant P values (<0.05).
Abbreviations: ISR, In-Stent Restenosis; CT-FFR, Computed tomography derived fractional flow reserve; FAI perivascular fat attenuation index.

and Model 2 (AUC: 0.923 vs 0.955, P < 0.05). The predictive value of ΔCT-FFR in combination with FAI is significantly greater than that of either parameter alone. There was no statistically significant difference between Model 2 and Model 3 (AUC: 0.955 vs 0.958, P > 0.05) (Figure 5 and Table 3). The calibration curve results show that most of the data points in the ISR prediction model are close to the ideal line, indicating that the model has a high degree of calibration (Figure 6). The results of the decision curve analysis show that in ISR prediction, the net gain of the model in most threshold probability ranges is higher than that under the assumption that all patients are positive or negative, indicating that the model has high clinical practicability (Figure 7).

Discussion

To the best of our knowledge, this is the first study to investigate the correlation between CT-FFR combined with FAI and its potential in predicting in-stent restenosis (ISR) in patients with coronary heart disease following percutaneous coronary intervention (PCI). Our findings demonstrate that ΔCT-FFR, CT-FFR$_{2cm}$, and peri-stent FAI derived from CCTA are moderately associated with ISR and may act as independent predictors for ISR after stent implantation.

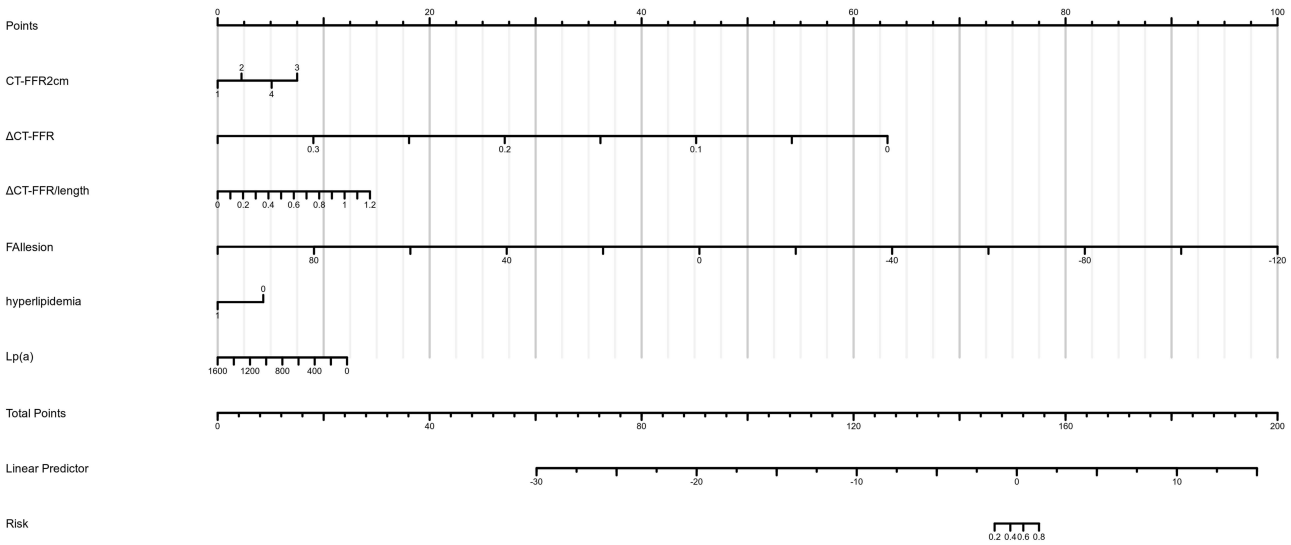

Figure 3 A nomogram model was developed to predict the occurrence of in-stent restenosis.

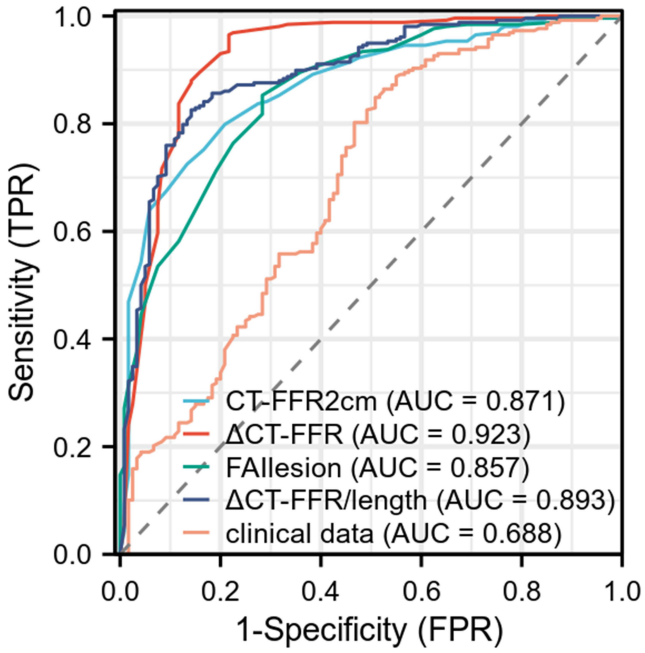

Figure 4 The receiver operating characteristic curves of each factor for predicting in-stent restenosis (ISR).

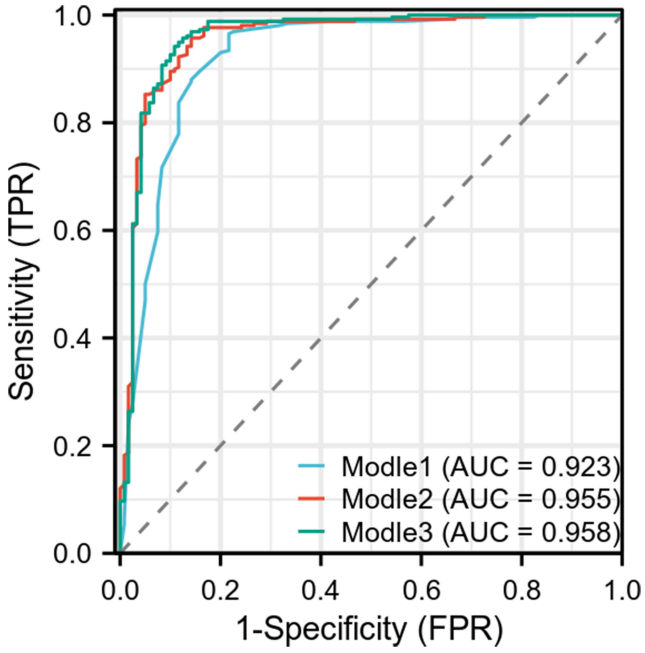

Figure 5 The receiver operating characteristic curves of each model for predicting in-stent restenosis.

Notably, while the integration of imaging features and clinical data enhances the identification of ISR, imaging features exhibit greater predictive value compared to clinical data alone.

Percutaneous coronary intervention initiates two distinct pathological processes that ultimately lead to ISR. In the early phase, ISR is primarily attributed to excessive neointimal hyperplasia, whereas in the later phase, it is predominantly caused by neoatherosclerosis.[25,26] Plaque rupture may further precipitate acute coronary syndrome and potentially result in major adverse cardiovascular events (MACE), including sudden cardiac death, thereby posing a significant threat to patient safety.[27] The fractional flow reserve (FFR) measured after PCI reflects the hemodynamic alterations in

https://doi.org/10.2147/TCRM.S554207

Table 3 The Results of the Work Characteristic Curves of ISR Predicted by Each Model

Characteristics	AUC	95% CI	Cut-Off value	Sensitivity	Specificity	Accuracy	PPV	NPV
Model 1	0.923	0.889–0.957	0.08	0.965	0.783	0.907	0.905	0.913
Model 2	0.955	0.930–0.981	0.439	0.957	0.858	0.926	0.936	0.904
Model 3	0.958	0.932–0.984	0.337	0.942	0.892	0.926	0.949	0.877

the target vessel where the stent is deployed. A lower FFR value indicates a reduced maximum blood flow capacity in the stented vessel under hyperemic conditions compared to a normal vessel, which may result in impaired blood flow, promote platelet aggregation and vascular occlusion, and consequently increase the risk and severity of ISR.[28] Conversely, a higher FFR level suggests favorable myocardial perfusion, adequate subendocardial oxygen supply, and diminished ischemia-induced inflammatory responses. These factors contribute to stable cellular metabolism, protection against ischemia-reperfusion injury, promotion of collateral circulation development, mitigation of adverse effects associated with vascular stenosis, and inhibition of ISR progression.[29,30] Previous studies have indicated that the FFR can serve as a valuable tool for assessing prognosis following PCI, with a significant post-PCI improvement in FFR being linked to greater symptom relief and a reduced incidence of adverse cardiovascular events.[9,31] Onuma et al[32] were the first to demonstrate the feasibility of using computational fluid dynamics (CFD)-based CT-derived FFR in patients undergoing PCI with bioabsorbable stents. Andreini et al[33] reported a case of severe ISR that was missed by coronary CT angiography but accurately detected by CT-FFR. In this case, CCTA did not detect significant stenosis within the RCA stent of the patient. On the contrary, CT-FFR analysis showed obvious distal stenosis of the RCA stent segment. Invasive coronary angiography confirmed severe ISR in RCA. Wang et al evaluated the predictive value of CT-FFR prior to PCI for target vessel failure (TVF) following stent implantation and found that CT-FFR, as an independent predictor of TVF, significantly improved risk reclassification compared with a clinical risk factor model.[34] Tang et al[13] were the first to investigate the predictive performance of machine learning (ML)-based CT-FFR for ISR. Their results indicated that CT-FFR achieved an accuracy rate of 85% in identifying ISR. During the follow-up period, statistically significant differences were observed between the ISR and non-ISR groups in terms of ΔCT-FFR and ΔCT-FFR/length. Moreover, ΔCT-FFR/length was identified as an independent predictor of ISR. In this study, statistically significant

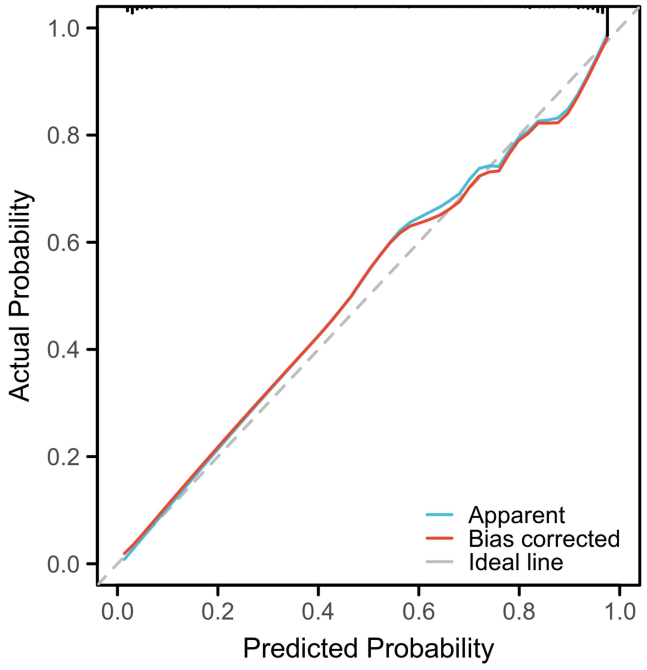

Figure 6 Calibration curves of each model for the prediction of in-stent restenosis.

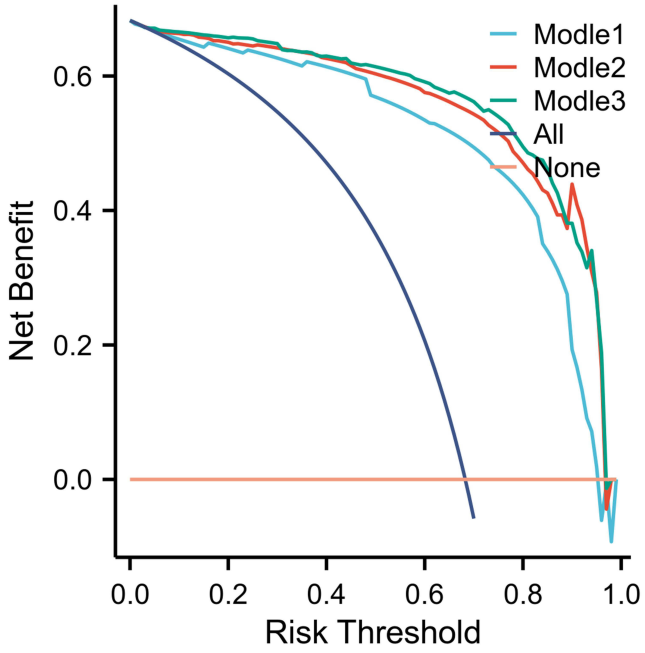

Figure 7 Decision curves of each model for the prediction of in-stem restenosis.

differences in CT-FFR$_{2cm}$, ΔCT-FFR, and ΔCT-FFR/length were found at each measured location between the two groups ($P < 0.05$), and CT-FFR$_{2cm}$, ΔCT-FFR, and ΔCT-FFR/length were all independently associated with ISR. These findings are largely consistent with those of previous studies. Furthermore, this study revealed that the predictive values of CT-FFR$_{2cm}$, ΔCT-FFR, and ΔCT-FFR/length for ISR were significantly higher than those of traditional risk factors such as hyperlipidemia and lipoprotein(a) [Lp(a)]. Therefore, we believe that for patients undergoing follow-up after PCI, it is essential to measure CT-FFR values at multiple locations within the stent, with particular emphasis on the difference in CT-FFR between the proximal and distal ends. As an independent predictor of ISR, ΔCT-FFR demonstrates high predictive accuracy for ISR assessment, significantly outperforming conventional clinical data.

Previous studies have confirmed that the development of ISR is closely associated with inflammatory processes.[35] Following stent implantation, vascular endothelial cells are damaged, and mechanical injury to the vascular wall triggers an inflammatory response. This inflammation promotes the formation of neointimal hyperplasia (NIH) and contributes to the development of neoatherosclerosis. Peri-coronary adipose tissue (PCAT) is capable of directly releasing substantial amounts of pro-inflammatory adipokines, cytokines, and chemokines, which contribute to endothelial dysfunction, inflammatory cell infiltration, and smooth muscle cell migration.[36,37] Additionally, mediators secreted from the inflamed vascular wall, such as interleukin-6 (IL-6), tumor necrosis factor-alpha (TNF-α), and plasminogen activator inhibitor-1 (PAI-1), can exert paracrine effects on PCAT. These mediators inhibit the proliferation and differentiation of human preadipocytes within PCAT, thereby suppressing lipid accumulation, reducing adipocyte numbers, and lowering overall lipid content.[38,39] Nogic et al initially examined the association between the mean attenuation of lesion-specific pericoronary adipose tissue (PCAT$_{lesion}$) prior to stent implantation and the occurrence of stent failure following PCI. Their findings indicated that PCAT$_{lesion}$ values were significantly elevated in patients who experienced stent failure compared to those who did not, and an increased PCAT$_{lesion}$ was identified as an independent predictor of stent failure.[23] The fat attenuation index, which is derived from CCTA, quantitatively assesses the CT attenuation gradient of PCAT, thereby reflecting the inflammatory activity of the coronary arteries and enabling non-invasive detection of coronary vascular inflammation. Adolf et al investigated the predictive significance of lesion-specific FAI (FAI$_{lesion}$) prior to stent placement with respect to in-stent restenosis (ISR). They found a significant correlation between FAI$_{lesion}$ and ISR, with elevated FAI$_{lesion}$ levels serving as an independent predictor of stent restenosis.[20] Qin et al first investigated the predictive value of peristent FAI for ISR and demonstrated that peristent FAI serves as an independent predictor of ISR, potentially functioning as a non-invasive biomarker for assessing the risk and severity of

https://doi.org/10.2147/TCRM.S554207

ISR following stent implantation.[40] These findings align with our research results. In our study, the lesion-specific peristent FAI (FAI_{lesion}) was significantly higher in the ISR group compared to the non-ISR group. As an independent predictor of ISR, FAI_{lesion} exhibited a moderate correlation with the occurrence of ISR. Moreover, the predictive value of FAI_{lesion} for ISR was found to be significantly greater than that of hyperlipidemia and lipoprotein(a) (Lp(a)). This study demonstrates that the FAI surrounding the stent, as a novel imaging biomarker of inflammation, holds significant clinical potential for the non-invasive assessment of ISR and may serve as a predictive tool for evaluating ISR risk following stent implantation. However, findings regarding the application value of FAI in ISR exhibit inconsistency. Another study evaluating the diagnostic value of radiomic features of pericoronary adipose tissue for in-stent restenosis reported no significant difference in peristent FAI between the ISR and non-ISR groups.[41] Therefore, the clinical utility of FAI in ISR requires comprehensive validation through large-scale clinical trials.

Limitations of this study include the following: (1) This was a single-center retrospective study, and selection bias may have occurred during patient enrollment. (2) The subjective editing of the stent vessel lumen profile could potentially influence subsequent CT-FFR and FAI calculations. Therefore, larger-scale and more comprehensive studies are required to further validate the clinical application of these parameters in the context of ISR. (3) Previous research has indicated that early and late in-stent restenosis involve distinct pathophysiological mechanisms.[42,43] However, this study did not differentiate between early and late ISR.

In conclusion, ΔCT-FFR and peri-stent FAI are independent predictors of in-stent restenosis following percutaneous coronary intervention, and demonstrate superior predictive performance for ISR compared to clinical characteristics. The combined application of these two parameters further enhances the predictive performance for ISR. The integration of CT-FFR and FAI techniques derived from CCTA enables a comprehensive and systematic evaluation of ISR through a "one-stop" assessment encompassing functional and inflammatory data. This non-invasive approach provides additional diagnostic value for ISR risk assessment: it not only helps reduce unnecessary invasive examinations in some patients and optimize the clinical management pathway for post-PCI ISR, but also lays a crucial foundation for individualized treatment decisions.

Data Sharing Statement

The datasets used or analyzed during the current study are available from the corresponding author on reasonable request.

Ethics Statement

This study was approved by the ethic committee of Linyi Central Hospital (LCH-LW-2025115) and it was carried out following the guidelines of the Helsinki Declaration (World Medical Association Declaration of Helsinki). Written informed consent was obtained from the patients for their participation in this study.

Disclosure

The authors declare that the research was conducted in the absence of any commercial or financial relationships that could be construed as a potential conflict of interest.

References

1. Khamis RY, Ammari T, Mikhail GW. Gender differences in coronary heart disease. *Heart*. 2016;102(14):1142–1149. doi:10.1136/heartjnl-2014-306463
2. Sulava EF, Johnson JC. Management of Coronary Artery Disease. *Surg Clin North Am*. 2022;102(3):449–464. doi:10.1016/j.suc.2022.01.005
3. Lawton JS, Tamis-Holland JE, Bangalore S, et al. Writing Committee Members. 2021 ACC/AHA/SCAI guideline for coronary artery revascularization: a report of the American college of cardiology/american heart association joint committee on clinical practice guidelines. *J Am Coll Cardiol*. 2022;79(2):e21–e129. doi:10.1016/j.jacc.2021.09.006
4. Madhavan MV, Kirtane AJ, Redfors B, et al. Stent-related adverse events >1 year after percutaneous coronary intervention. *J Am Coll Cardiol*. 2020;75(6):590–604. doi:10.1016/j.jacc.2019.11.058
5. Kawai K, Virmani R, Finn AV. In-Stent Restenosis. *Interv Cardiol Clin*. 2022;11(4):429–443. doi:10.1016/j.iccl.2022.02.005
6. Kufner S, Joner M, Thannheimer A, et al. Ten-year clinical outcomes from a trial of three limus-eluting stents with different polymer coatings in patients with coronary artery disease. *Circulation*. 2019;139:325–333. doi:10.1161/CIRCULATIONAHA.118.038065
7. Seiler T, Attinger-Toller A, Cioffi GM, et al. Treatment of in-stent restenosis using a dedicated super high-pressure balloon. *Cardiovasc Revasc Med*. 2023;46:29–35. doi:10.1016/j.carrev.2022.08.018

8. Cuesta J, Pérez-Vizcayno MJ, García Del Blanco B, et al. Long-term results of bioresorbable vascular scaffolds in patients with in-stent restenosis: the RIBS VI study. *JACC Cardiovasc Interv*. 2024;17(15):1825–1836.
9. Frøbert O, Götberg M. Fractional flow reserve-dichotomous decisions in myocardial ischemia. *Circ Cardiovasc Interv*. 2022;15(2):e011787. doi:10.1161/CIRCINTERVENTIONS.122.011787
10. BKrüger S, Koch KC, Kaumanns I, et al. Use of fractional flow reserve versus stress perfusion scintigraphy in stent restenosis. *Eur J Intern Med*. 2005;16(6):429–431. doi:10.1016/j.ejim.2005.01.022
11. Nørgaard BL, Leipsic J, Gaur S, et al. NXT Trial Study Group. Diagnostic performance of noninvasive fractional flow reserve derived from coronary computed tomography angiography in suspected coronary artery disease: the NXT trial (Analysis of coronary blood flow using CT angiography: next steps). *J Am Coll Cardiol*. 2014;63(12):1145–1155. doi:10.1016/j.jacc.2013.11.043
12. Kawase Y, Matsuo H, Kuramitsu S, et al. Clinical use of physiological lesion assessment using pressure guidewires: an expert consensus document of the Japanese association of cardiovascular intervention and therapeutics-update 2022. *Cardiovasc Interv Ther*. 2022;37(3):425–439. doi:10.1007/s12928-022-00863-1
13. Tang CX, Guo BJ, Schoepf JU, et al. Feasibility and prognostic role of machine learning-based FFRCT in patients with stent implantation. *Eur Radiol*. 2021;31(9):6592–6604. doi:10.1007/s00330-021-07922-w
14. Farag SI, Mostafa SA, El-Rabbat KE, El-Kaffas SM, Awara DM. The relation between pericoronary fat thickness and density quantified by coronary computed tomography angiography with coronary artery disease severity. *Indian Heart J*. 2023;75(1):53–58. doi:10.1016/j.ihj.2023.01.006
15. Oikonomou EK, Marwan M, Desai MY, et al. Non-invasive detection of coronary inflammation using computed tomography and prediction of residual cardiovascular risk (the CRISP CT study): a post-hoc analysis of prospective outcome data. *Lancet*. 2018;392(10151):929–939. doi:10.1016/S0140-6736(18)31114-0
16. Guo B, Jiang M, Guo X, et al. Diagnostic and prognostic performance of artificial intelligence-based fully-automated on-site CT-FFR in patients with CAD. *Sci Bull*. 2024;69(10):1472–1485. doi:10.1016/j.scib.2024.03.053
17. Von Knebel Doeberitz PL, De Cecco CN, Schoepf UJ, et al. Coronary CT angiography-derived plaque quantification with artificial intelligence CT fractional flow reserve for the identification of lesion-specific ischemia. *Eur Radiol*. 2019;29(5):2378–2387. doi:10.1007/s00330-018-5834-z
18. Zhang R, Ju Z, Li Y, Gao Y, Gu H, Wang X. Pericoronary fat attenuation index is associated with plaque parameters and stenosis severity in patients with acute coronary syndrome: a cross-sectional study. *J Thorac Dis*. 2022;14(12):4865–4876. doi:10.21037/jtd-22-1536
19. Yu Y, Shan D, Wang X, et al. Predictive value of the perivascular fat attenuation index for MACE in young people suspected of CAD. *BMC Cardiovasc Disord*. 2025;25(1):80. doi:10.1186/s12872-024-04401-0
20. Adolf R, Krinke I, Datz J, et al. Specific calcium deposition on pre-procedural CCTA at the time of percutaneous coronary intervention predicts in-stent restenosis in symptomatic patients. *J Cardiovasc Comput Tomogr*. 2025;19(1):9–16. doi:10.1016/j.jcct.2024.09.010
21. Jensen JM, Bøtker HE, Mathiassen ON, et al. Computed tomography derived fractional flow reserve testing in stable patients with typical angina pectoris: influence on downstream rate of invasive coronary angiography. *Eur Heart J Cardiovasc Imaging*. 2018;19(4):405–414. doi:10.1093/ehjci/jex068
22. Kueh SH, Mooney J, Ohana M, et al. Fractional flow reserve derived from coronary computed tomography angiography reclassification rate using value distal to lesion compared to lowest value. *J Cardiovasc Comput Tomogr*. 2017;11(6):462–467. doi:10.1016/j.jcct.2017.09.009
23. Nogic J, Kim J, Layland J, et al. Peri-coronary adipose tissue is a predictor of stent failure in patients undergoing percutaneous coronary intervention. *Cardiovasc Revasc Med*. 2023;53:61–66. doi:10.1016/j.carrev.2023.02.022
24. Kuntz RE, Baim DS. Defining coronary restenosis. Newer clinical and angiographic paradigms. *Circulation*. 1993;88(3):1310–1323. doi:10.1161/01.cir.88.3.1310
25. Otsuka F, Byrne RA, Yahagi K, et al. Neoatherosclerosis: overview of histopathologic findings and implications for intravascular imaging assessment. *Eur Heart J*. 2015;36(32):2147–2159. doi:10.1093/eurheartj/ehv205
26. Pelliccia F, Zimarino M, Niccoli G, et al. In-stent restenosis after percutaneous coronary intervention: emerging knowledge on biological pathways. *Eur Heart J Open*. 2023;3(5):oead083. PMID: 37808526; PMCID: PMC10558044. doi:10.1093/ehjopen/oead083
27. Sakamoto A, Sato Y, Kawakami R, et al. Risk prediction of in-stent restenosis among patients with coronary drug-eluting stents: current clinical approaches and challenges. *Expert Rev Cardiovasc Ther*. 2021;19(9):801–816. doi:10.1080/14779072.2021.1856657
28. McInerney A, Travieso Gonzalez A, Castro Mejía A, et al. Long-term outcomes after deferral of revascularization of in-stent restenosis using fractional flow reserve. *Catheter Cardiovasc Interv*. 2022;99(3):723–729. doi:10.1002/ccd.29823
29. Erdoğan M, Erdöl MA, Öztürk S, Durmaz T. Systemic immune-inflammation index is a novel marker to predict functionally significant coronary artery stenosis. *Biomarker Med*. 2020;14(16):1553–1561. doi:10.2217/bmm-2020-0274
30. le Noble F, Kupatt C. Interdependence of angiogenesis and arteriogenesis in development and disease. *Int J Mol Sci*. 2022;23(7):3879. doi:10.3390/ijms23073879
31. Hirai K, Kawasaki T, Sakakura K, et al. Determinants of insufficient improvement in fractional flow reserve following percutaneous coronary intervention. *Heart Vessels*. 2020;35(12):1650–1656. doi:10.1007/s00380-020-01645-6
32. Onuma Y, Collet C, van Geuns RJ, et al. ABSORB investigators. Long-term serial non-invasive multislice computed tomography angiography with functional evaluation after coronary implantation of a bioresorbable everolimus-eluting scaffold: the ABSORB cohort B MSCT substudy. *Eur Heart J Cardiovasc Imaging*. 2017;18(8):870–879. doi:10.1093/ehjci/jex022
33. Andreini D, Mushtaq S, Pontone G, Rogers C, Pepi M, Bartorelli AL. Severe in-stent restenosis missed by coronary CT angiography and accurately detected with FFRCT. *Int J Cardiovasc Imaging*. 2017;33(1):119–120. doi:10.1007/s10554-016-0971-4
34. Wang Z, Tang C, Zuo R, et al. Pre-PCI CT-FFR predicts target vessel failure after stent implantation. *J Thorac Imaging*. 2024;39(4):232–240. doi:10.1097/RTI.0000000000000791
35. Pepe M, Napoli G, Carulli E, et al. Autoimmune diseases in patients undergoing percutaneous coronary intervention: a risk factor for in-stent restenosis? *Atherosclerosis*. 2021;333:24–31. doi:10.1016/j.atherosclerosis.2021.08.007
36. Fernández-Alfonso MS, Gil-Ortega M, García-Prieto CF, Aranguez I, Ruiz-Gayo M, Somoza B. Mechanisms of perivascular adipose tissue dysfunction in obesity. *Int J Endocrinol*. 2013;2013:402053. doi:10.1155/2013/402053
37. Oguz M, Akbulut T, Saylik F, Sipal A, Erdal E. Association of coronary artery severity and late in-stent restenosis: an angiographic imaging study. *Angiology*. 2024;75(2):122–130. doi:10.1177/00033197221150953

38. Antonopoulos AS, Simantiris S. Detecting the vulnerable patient: toward preventive imaging by coronary computed tomography angiography. *Circ Cardiovasc Imaging*. 2023;16(2):e015135. doi:10.1161/CIRCIMAGING.122.015135
39. Antonopoulos AS, Sanna F, Sabharwal N, et al. Detecting human coronary inflammation by imaging perivascular fat. *Sci Transl Med*. 2017;9(398): eaal2658. doi:10.1126/scitranslmed.aal2658
40. Qin B, Li Z, Zhou H, Liu Y, Wu H, Wang Z. The predictive value of the perivascular adipose tissue CT fat attenuation index for coronary in-stent restenosis. *Front Cardiovasc Med*. 2022;9:822308. doi:10.3389/fcvm.2022.822308
41. Cui K, Liang S, Hua M, et al. Diagnostic performance of machine learning-derived radiomics signature of pericoronary adipose tissue in coronary computed tomography angiography for coronary artery in-stent restenosis. *Acad Radiol*. 2023;30(12):2834–2843. doi:10.1016/j.acra.2023.04.006
42. Jinnouchi H, Kuramitsu S, Shinozaki T, et al. Difference of tissue characteristics between early and late restenosis after second-generation drug-eluting stents implantation- an optical coherence tomography study. *Circ J*. 2017;81(4):450–457. doi:10.1253/circj.CJ-16-1069
43. Feng C, Zhang P, Han B, et al. Optical coherence tomographic analysis of drug-eluting in-stent restenosis at different times: a STROBE compliant study. *Medicine*. 2018;97(34):e12117. PMID: 30142870; PMCID: PMC6372013. doi:10.1097/MD.0000000000012117